Towards High Speed Bearingless Drives

Hubert Mitterhofer[1,a], Wolfgang Amrhein[1,b], Wolfgang Gruber[1,c]
[1]Institute for Electrical Drives and Power Electronics
Johannes Kepler University Linz, Austria
Shareholder of the ACCM GmbH
[a]hubert.mitterhofer@jku.at, [b]wolfgang.amrhein@jku.at, [c]wolfgang.gruber@jku.at

Abstract: The design of a high speed bearingless drive shows special requirements concerning topology and loss minimization. This paper discusses the use of a bearingless disc motor for such a purpose. The effects of the selected geometric dimensions on the ability to produce passive and active bearing forces are studied in 3D-FEM simulations. Furthermore, a toroid winding, suitable for the chosen flat motor geometry, and an adequate 5-phase winding scheme are proposed. In an analytical part, the copper losses due to the motor and bearing currents, as well as due to the external rotor magnet field are calculated. The results lead to the selection of a preferable litz wire gauge which is finally used in the construction of a first motor prototype.

Keywords: Bearingless Drive, Disc Motor, Toroid Winding, Eddy Current Losses, Skin Effect, Proximity Effect, Litz Wire

Introduction

Over the past decade, the development in magnetic bearing technology has drawn great interest worldwide. In addition to the well known advantages of magnetic bearings, great advances in drive compactness and material costs can be achieved by placing the motor and bearing unit onto one common stator. Going even further, the winding systems can be combined, too. This results in a highly concentrated design, where each coil contributes to both bearing forces and motor torque. In analogy to the term *sensorless*, these emerging drives are referenced as *bearingless* drives.
A favorable form of implementation are disc motors. These motors use the passive stabilization of magnetically suspended slice rotors for the axial and the two tilt deflections (Fig. 1). Thus, the active stabilization degrees are reduced to the two radial deflections only. So far, bearingless

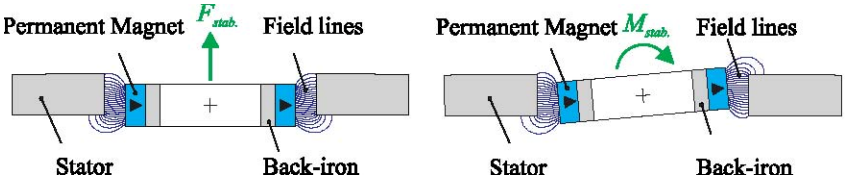

Fig. 1. Passive stabilization of disc motors

disc drives have mostly been implemented to be suitable for pumps [1]–[8] and special equipment as, e.g., in biotechnology or semiconductor processing [9]–[11]. As shown in Fig. 2 the required rotational speeds typically do not need to exceed 15.000rpm.
Some of the main difficulties when pushing for high rotational speeds are the magnetic bearing properties and the rotordynamic stability. Furthermore, various losses such as eddy current losses increase with rising speed and, therefore, need to be minimized. Addressing the various difficulties throughout the design process, the presented paper discusses principle aspects for high speed bearingless drives.

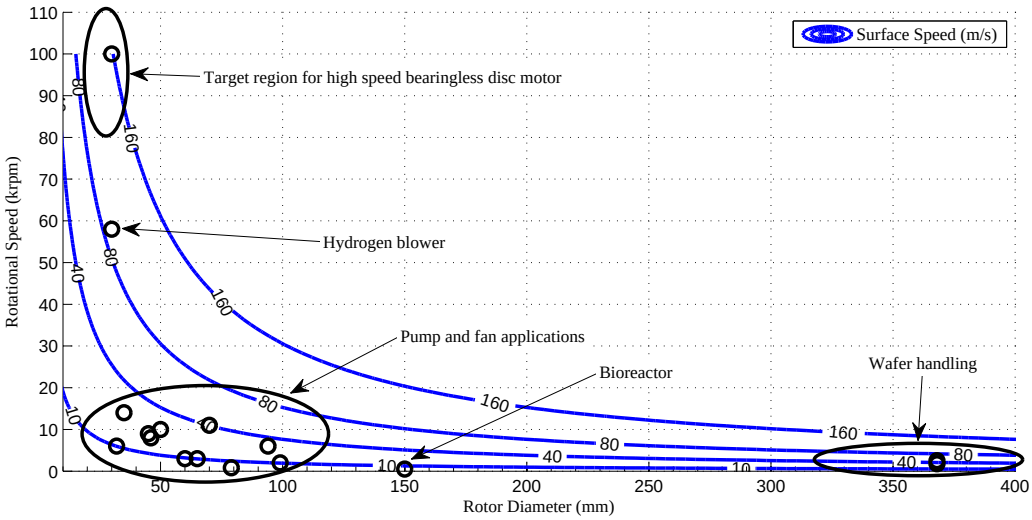

Fig. 2. Map of bearingless drives

Drive Design

Motor Topology: The interior rotor PMSM design applied in this project uses a diametrically magnetized NdFeB magnet ring in order to produce a smooth sinusoidal magnetic field in the air gap. Fig. 3 shows the magnetic field lines when using a sintered N42 NdFeB permanent magnet ring rotor with an inner back iron ring. This hollow ring structure allows a higher ratio of polar (J_p) to diametrical (J_d) moment of inertia without reducing the axial length l_r and thus, the producible bearing forces and torques, because

$$\frac{J_p}{J_d} = 2 \cdot \frac{(r_o^2 + r_i^2)}{(r_o^2 + r_i^2 + \frac{l_r^2}{3})}. \tag{1}$$

m_r, r_{r_o} and r_{b_i} represent the rotor mass, its outer diameter and the inner radius of the back iron ring, respectively.

Winding design: The stator made of laminated nickel-iron alloy carries a star-connected 5-phase slotless winding system constituting the minimum number of phases necessary for both controlling motor torque and bearing forces independently and avoiding single-phase characteristic when using a slotless motor [12]. Furthermore, the slotless design reduces the hysteresis and eddy current losses in the stator, which are especially relevant at high rotational speeds of the rotor.
With the chosen configuration of 5 phases and 1 coil per phase, only 3 winding variants shown in Fig. 5 are feasible. Of these three possibilities, the full-pitch winding (Fig. 5(a)) cannot generate any bearing force on a diametrically magnetized magnet rotor. The winding system with concentrated coils (Fig. 5(c)) has a winding factor of only 0.587 for creating the magnetic field necessary for generating torque. With the remaining variant (Fig. 5(b)), this value is 0.951, which means it is better suited to create torque-generating magnetic fields. The capabilities to produce bearing forces with the latter two systems are exactly opposite: 0.951 for system (c) and 0.587 for (b). For the first prototype, system (b) is chosen, since even the smaller bearing forces will satisfy the requirements according to 3D-FEM simulations and a better efficiency can be expected.

Winding form: Instead of a conventional air gap winding, a toroid winding form as shown in Fig. 4 is used. Basically, these two coil types are equivalent concerning torque and bearing force creation [13] but still the toroid form is very unusual for motors. First, the ratio of winding head to active coil length increases for the toroid, and decreases for the conventional air gap winding with

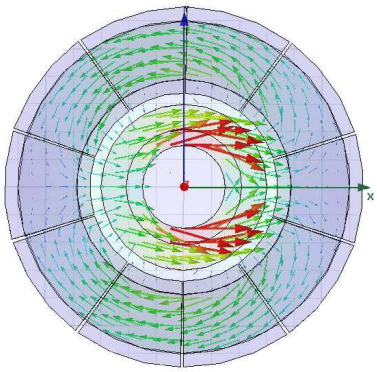

Fig. 3. 3D FEM magnetic field computation

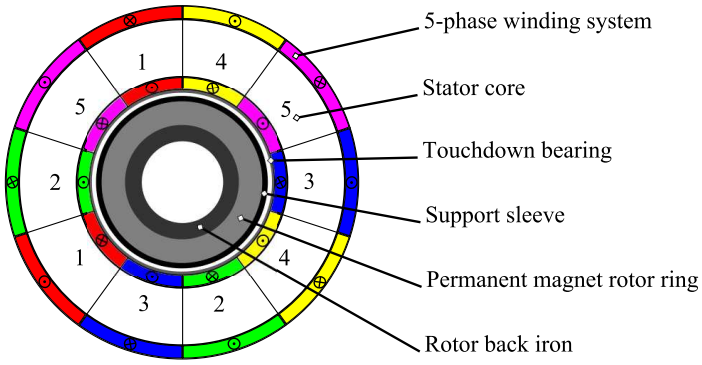

Fig. 4. 5-phase toroid winding

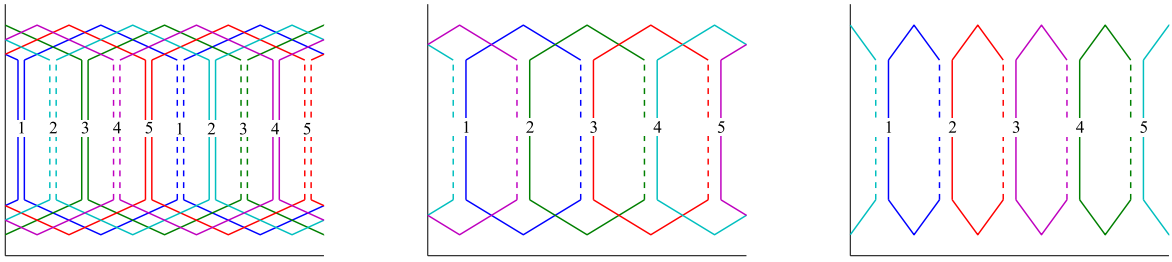

(a) Full-pitch windings (b) Reduced-pitch windings (c) Concentrated windings

Fig. 5. Possible winding schemes

rising axial motor length. Second, the toroid form leads to a significant increase of wire length in case of concentrated coils. However, in the present flat motor design with the chosen winding configuration (b) the necessary wire length is reduced by 21% due to shorter end windings, thus decreasing resistive losses. Also, the toroid winding form is much easier to manufacture and more flexible in the sense of a modular prototype.

Wire selection: Despite its advantages concerning iron losses, the slotless design means that the alternating magnetic rotor field is not concentrated in stator teeth but is penetrating the copper conductors, where eddy currents are induced. Concerning transformers, [14]–[17] deal with analytical approaches to calculate the AC-related winding losses. Ferraras separation approach due to orthogonality [17] can be written as

$$P_{skin} = N_s \cdot R_{dc,s} \cdot l_{wire} \cdot F_{skin} \cdot (\frac{\hat{I}}{N_s})^2 \tag{2}$$

for skin effect related losses and

$$P_{prox} = N_s \cdot R_{dc,s} \cdot l_{wire} \cdot G_{prox} \cdot (\frac{\hat{I}^2}{2 \cdot \pi^2 \cdot d_w^2} + \hat{H}^2)) \tag{3}$$

with l_{wire} being the wire length, N_s the number of strands in case of litz wire and $R_{dc,s}$ the resistance per unit length of the wire in case a solid conductor and of one strand in case of litz wire. Further, d_w represents the diameter of the entire litz bundle or the solid wire. $\hat{I}$ stands for the peak value of the applied sinus current and $\hat{H}$ is the peak value of the cumulated magnetic field due to the neighboring wires. The exact formulation of F_{skin} and G_{prox} is only possible for round conductors. They yield

$$F_{skin} = \frac{\xi}{4} \cdot \frac{KelvinBer(0,\xi) \cdot KelvinBei'(0,\xi) - KelvinBei(0,\xi) \cdot KelvinBer'(0,\xi)}{KelvinBer'(0,\xi)^2 + KelvinBei'(0,\xi)^2}, \tag{4}$$

$$G_{prox} = \frac{\xi \cdot \pi^2 \cdot d_s^2}{2} \cdot \frac{KelvinBer(2,\xi) \cdot KelvinBer'(0,\xi) + KelvinBei(2,\xi) \cdot KelvinBei'(0,\xi)}{KelvinBer'(0,\xi)^2 + KelvinBei'(0,\xi)^2}, \tag{5}$$

with

$$\xi = \frac{d_s}{\sqrt{2} \cdot \delta} \tag{6}$$

where d_s and δ represent the strand diameter and the skin depth of the concerned strand or solid wire. $KelvinBer$ and $KelvinBei$ stand for the real and imaginary part of the Kelvin differential equation describing a Bessel function of the first kind.
The above calculation scheme can be adapted to calculate the losses occurring in the copper windings of the presented motor. Skin effect losses describe the copper losses as a function of the applied frequency. At the present maximum frequency, however, the resistance increase is below 0.2% for the solid wire and below $0.5 \cdot 10^{-3}\%$ for the litz wires. Therefore, the skin effect related losses can be approximated as being equivalent to the DC-copper losses.
The internal proximity effect is only relevant for litz wires, since it describes the eddy currents due to the magnetic field produced by the neighboring strands within the same wire. The external proximity effect however, takes the eddy currents, provoked by the magnetic field of the neighboring wires ($\hat{H}_w$), into account. Other components, such as the magnetic field due to a nearby permanent magnet ($\hat{H}_e$), can also be superposed as long as they can also be estimated to be uniform within the regarded conductor. Eq.7 gives the description of the total losses in the 5-phase motor winding.

$$P_{total} = 5 \cdot N_s \cdot R_{dc,s} \cdot l_{wire} \cdot (F_{skin} \cdot (\frac{\hat{I}}{Ns})^2 + G_{prox} \cdot (\frac{\hat{I}^2}{2 \cdot \pi^2 \cdot d_w^2} + (\hat{H}_w + \hat{H}_e)^2)), \tag{7}$$

The internal proximity effect as well as the external proximity effect due to the neighboring wires turn out to be absolutely negligible due to the low frequencies - the losses due to these effects are in the sub-mW range. Therefore, just the DC-losses and the proximity effect due to the external permanent magnetic field are relevant. Fig. 6 shows the DC-losses and the total prospective losses

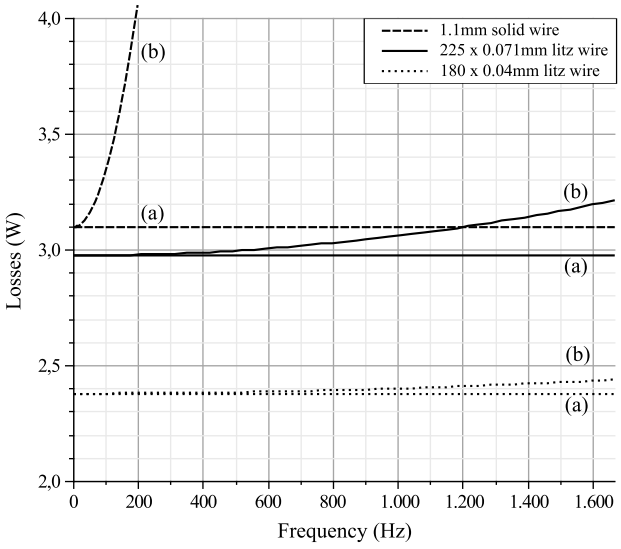

Fig. 6. DC-losses considering skin effect (a) and total losses (b) for 3 wire types

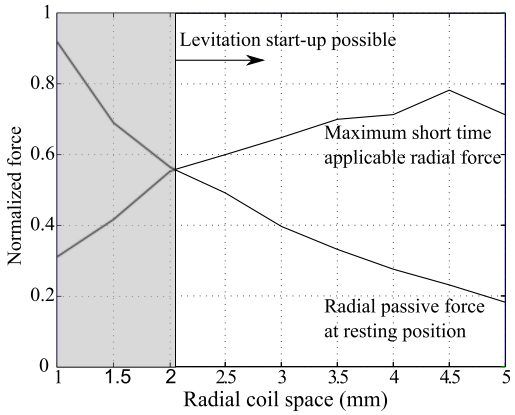

Fig. 7. Radial stiffness vs. Possible start-up forces

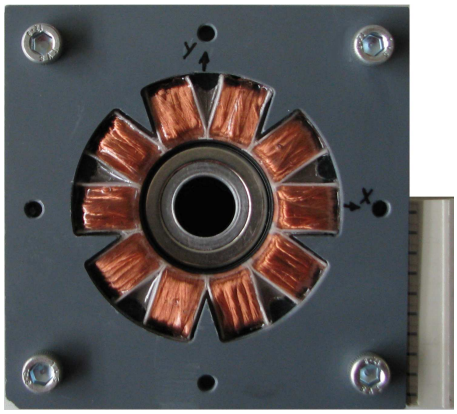

Fig. 8. Prototype motor

for two different litz wire and one solid wire configuration, respectively. Also, Fig. 6 clearly shows that the proximity effect losses for the solid wire become very high as the rotational speed increases. Litz wire is therefore used instead of solid wire.
It is assumed that all the conductors which are connected in parallel, such as the single strands of a litz wire, experience the same flux linkage. This would otherwise lead to different induced voltages within single strands and resulting balancing currents causing additional copper losses. In order to keep this effect as low as possible, the litz wire needs to be twisted, so that each conductor preferably experiences the same induced voltage.

3D-FEM Calculation

Several requirements concerning the motor characteristics can be linked to distinct geometric dimensions. First, the ratio of polar to diametrical moment of inertia of the rotor must be kept above 1 to constitute the rotational axis as principal axis of inertia in order to ensure proper rotordynamic behavior. Then, the passive stabilization forces for axial and tilt deflection can be increased by reducing the magnetic air gap and the axial motor length. However, the available winding space must remain wide enough to allow the production of the necessary torques and radial forces without having to apply unacceptably high current densities to the windings. This concerns not only normal motor operation, where the limit for the permanently applicable current density was set to $5\frac{A}{mm^2}$ but also the start-up procedure. For the short period of time, necessary to lift the rotor out of its excentric resting position, the current limit is given by the power electronics. The above demands were used as target parameters for the conducted 3D-FEM optimization as a 2D finite element simulation would not take the winding head and other edge effects into account that are relevant for flat motor geometries. Fig. 7 shows the FEM results for the radial passive forces acting on the rotor in the resting position and the short term maximum of the producible radial active bearing forces. The latter increase proportionally with available coil space, but saturate due to decreasing magnetic field strength, since the coil space is part of the magnetic air gap in the present slotless motor design.

Prototype

A first prototype, which is shown in Fig. 8, implements the conclusions of the analytical and FEM supported design process. The wire selection was influenced by a limitation concerning available phase voltages. In drives using separated motor and magnetic bearing units, the torque-winding experiences the back-EMF induced by the alternating rotor field. This reduces the voltage range available and thus limits the current transition rate. With only one combined winding system present in the proposed design, the creation of both torque and bearing forces is concerned. Therefore, the

$225 \times 0.071mm$ litz wire was used for the prototype coil system. Even though it yields higher losses than the $180 \times 0.04mm$ wires, the coils feature less winding turns, which limits the induced back-EMF and allows proper levitation up to the target speed.

Conclusion and outlook

This paper presents the layout of a slotless 5-phase bearingless disc drive suitable for high speed operation. The dependencies between geometric dimensions and the producible passive and active magnetic bearing forces show that the values for, e.g. axial motor length, coil space width and magnetic air gap width have to be chosen thoughtfully in order to permit the functionality of the bearing unit. In 3D-FEM simulations, the assumed dependencies are analyzed and verified. Furthermore, a special focus is put on the winding design, where a toroid winding form is proposed. In an analytical calculation of the eddy current losses, it is shown that litz wire should be used instead of solid wire in order to minimize the occurring losses due to the rotating permanent magnetic field of the rotor. Following the results of the simulation and analytical calculation results, a first prototype has been built. In the next design state, measurements have to be conducted in order to verify the loss predictions and design decisions.

Acknowledgment

This work is conducted within the strategic research program at the Austrian Center of Competence in Mechatronics (ACCM), which is a part of the COMET K2 program of the Austrian Government. The projects are kindly supported by the Austrian Government, the Upper Austrian Government and the Johannes Kepler University Linz. The authors thank all involved partners for their support.

References

[1] K. Raggl, B. Warberger, T. Nussbaumer, S. Burger, and J. W. Kolar, "Robust angle-sensorless control of a pmsm bearingless pump," *IEEE Transactions on Industrial Electronics*, vol. 56, no. 6, pp. 2076–2085, 2009.

[2] J. Asama, A. Chiba, T. Oiwa, T. Fukao, and A. Rahman, "A design consideration of a novel bearingless disk motor for artificial hearts," *Proc. on 1st IEEE Energy Conversion Congress and Exposition*, pp. 1693–1699, 2009.

[3] S. Wan, K. J. Tseng, and W. K. Chan, "Novel bearingless centrifugal blood pump," in *Proc. on 4th IEEE Int. Conf. on Power Electronics and Drive Systems*, 2001, pp. 743–748.

[4] M. Ooshima and C. Takeuchi, "Magnetic suspension performance of a bearingless brushless dc motor for small liquid pumps," in *Proc. on 12th ICEMS Int. Conf. on Electrical Machines and Systems*, 2009, pp. 1–4.

[5] W. Gruber, W. Amrhein, and M. Haslmayr, "Bearingless segment motor with five stator elements – design and optimization," *IEEE Transactions on Industry Applications*, vol. 45, no. 4, pp. 1301–1308, 2009.

[6] R. Baumschlager, R. Schöb, and J. Schmied, "Bearingless hydrogen blower," in *Proc. on 8th ISMB Int. Symposium on Magnetic Bearings*, 2002.

[7] T. Nussbaumer, K. Raggl, P. Boesch, and J. W. Kolar, "Trends in integration for magnetically levitated pump systems," in *Proc. on 4th PCC Power Conversion Conference*, 2007, pp. 1551–1558.

[8] T. Reichert, T. Nussbaumer, W. Gruber, and J. W. Kolar, "Design of a novel bearingless permanent magnet motor for bioreactor applications," in *35th IEEE Conf. Industrial Electronics*, 2009, pp. 1086–1091.

[9] F. Zürcher, T. Nussbaumer, W. Gruber, and J. W. Kolar, "Design and development of a 26-pole and 24-slot bearingless motor," *IEEE Transactions on Magnetics*, vol. 45, no. 10, pp. 4594–4597, 2009.

[10] W. Gruber, T. Nussbaumer, H. Grabner, and W. Amrhein, "Wide air gap and large-scale bearingless segment motor with six stator elements," *IEEE Transactions on Magnetics*, vol. 46, no. 6, pp. 2438–2441, 2010.

[11] T. Schneeberger, T. Nussbaumer, and J. W. Kolar, "Magnetically levitated homopolar hollow-shaft motor," *IEEE/ASME Transactions on Mechatronics*, vol. 15, no. 1, pp. 97–107, 2010.

[12] H. Grabner, W. Amrhein, S. Silber, and W. Gruber, "Nonlinear feedback control of a bearingless brushless dc motor," *IEEE/ASME Transactions on Mechatronics*, vol. 15, no. 1, pp. 40–47, 2010.

[13] R. Nakamura, K. Kamiya, A. Chiba, J. Asama, and T. Fukao, "Stator design of a multi-consequent-pole bearingless motor with toroidal winding," in *Proc. on 1st IEEE Energy Conversion Congress and Exposition*, 2009, pp. 2403–2408.

[14] J. A. Ferreira, "Analytical computation of ac resistance of round and rectangular litz wire windings," *IEE Proceedings - B*, vol. 139, no. 1, pp. 21–25, 1992.

[15] F. Tourkhani and P. Viarouge, "Accurate analytical model of winding losses in round litz wire windings," *IEEE Transactions on Magnetics*, vol. 37, no. 1, pp. 538–543, 2001.

[16] C. R. Sullivan, "Optimal choice for number of strands in a litz-wire transformer winding," *IEEE Transactions on Power Electronics*, vol. 14, no. 2, pp. 283–291, 1999.

[17] J. A. Ferreira, "Improved analytical modeling of conductive losses in magnetic components," *IEEE Transactions on Power Electronics*, vol. 9, no. 1, pp. 127–131, 1994.